GJETA

Global Journal of Engineering and Technology Advances

eISSN: 2582-5003

Cross Ref DOI: 10.30574/gjeta

Journal homepage: https://gjeta.com/

Global Journal of Engineering and Technology Advances

Global Scholar Press, INDIA

(Research Article)

Check for updates

REAL-TIME ESTIMATION OF ROCKET MOTOR PERFORMANCE USING MULTI-SENSOR FUSION AND AN ADAPTIVE KALMAN FILTER

Solomon saiki [1,*], Abimaje Shedrach Olobo [2], Engr Alli Adebayo Matthew [3], Engr Hassan yunusa Ibrahim [4] and Ahmed Abdulrahman Yakubu [5]

[1] Department of rocket engine system BATCSTP/NASRDA.
[2] Department of rocket propulsion system BATCSTP/NASRDA.
[2] Department of thrust engine system BATCSTP/NASRDA.
[4] Department of maintenance and infrastructure BATCSTP/ NASRDA.
[5] Department of rocket stability and recovery system BATCSTP/NASRDA.
* Corresponding Author

Global Journal of Engineering and Technology Advances, 2026, 28(03), 053–063

Publication history: Received on 18 July 2026; revised on 30 August 2026; accepted on 01 September 2026

Article DOI: https://doi.org/10.30574/gjeta.2026.28.3.0232

ABSTRACT

Ground and flight testing of solid-propellant rocket motors requires accurate, low-latency knowledge of chamber pressure, thrust, and specific impulse (I_{sp}), yet no single instrumentation channel provides all three with adequate bandwidth and noise immunity. This paper presents a real-time multi-sensor fusion architecture that combines a chamber-pressure transducer, a thrust load cell, and an axial accelerometer-derived thrust channel through a discrete Kalman filter with innovation-based adaptive process noise (IAE). The adaptive mechanism inflates the process-noise covariance for a short, bounded interval whenever the normalized innovation exceeds a threshold, allowing the filter to track the fast ignition and tail-off transients of a solid-motor burn without sacrificing steady-state noise rejection during the quasi-steady burn phase. The approach is validated against a physically grounded internal-ballistics truth model of an AP/HTPB/aluminized composite motor (Saint-Robert burn law, chamber-filling dynamics, choked-nozzle thrust with correct exit-pressure correction) corrupted with realistic transducer, load-cell, and accelerometer noise. The fused estimator reduces chamber-pressure RMS error by 22.2% and thrust RMS error by 39.0% relative to the raw sensor channels, and reconstructs real-time specific impulse to within 0.02% of the true burn-averaged value during the quasi-steady phase. The results indicate that adaptive multi-sensor fusion is a practical, low-cost path to real-time motor-performance telemetry suitable for static test stands, abort-decision logic, and small-scale flight avionics.

Keyword*:* Sensor Fusion, Kalman Filter, Solid Rocket Motor, Specific Impulse, Real-Time Estimation, Chamber Pressure, Thrust Measurement, Adaptive Filtering.

1 INTRODUCTION

Static and flight testing of solid rocket motors relies on accurate, time-resolved measurement of chamber pressure P_c, thrust F, and derived performance metrics such as characteristic velocity c^* and specific impulse I_{sp}. These quantities are conventionally reconstructed by post-processing logged sensor data after a static fire, which is adequate for after-action performance verification but precludes real-time use in abort logic, adaptive thrust-vector control, or in-flight health monitoring. A pressure transducer and a load cell each measure a different physical quantity with different bandwidth, noise character, and failure modes; neither channel alone gives a complete, noise-robust picture of instantaneous motor performance.

Multi-sensor fusion — the combination of redundant or complementary sensor channels through a statistically optimal estimator — is well established in inertial navigation and attitude determination [1], [2], where MEMS gyroscopes, accelerometers, and magnetometers are fused with a Kalman filter to obtain a smoother, lower-latency state estimate than any individual sensor provides. The same principle applies naturally to propulsion instrumentation: a chamber-pressure transducer and a thrust load cell are physically coupled through the nozzle relation $F = C_f P_c A_t$, so fusing them allows each channel to compensate for the other's noise and transient response.

A central difficulty in applying a fixed-gain Kalman filter to motor-performance estimation is that the underlying signal is highly non-stationary: chamber pressure and thrust rise over tens of milliseconds at ignition, remain quasi-steady for seconds during the sustained burn, and fall rapidly at tail-off as the propellant grain is consumed. A filter tuned for good noise rejection during the steady burn lags badly during the ignition and tail-off transients; a filter tuned for fast transient tracking under-rejects sensor noise during the steady phase. This paper addresses that trade-off with an innovation-based adaptive estimation (IAE) scheme [11], [12] that temporarily inflates the process-noise covariance whenever the filter's normalized innovation exceeds a threshold, then relaxes back to tightly tuned steady-burn values.

The contributions of this paper are threefold: (1) a compact multi-sensor fusion architecture for real-time rocket-motor performance estimation combining chamber pressure, thrust, and an independent accelerometer-derived thrust channel; (2) an adaptive Kalman filter formulation that resolves the transient-tracking/noise-rejection trade-off without increasing state-vector dimensionality; and (3) a simulation-based validation against a physically consistent internal-ballistics truth model, quantifying the achievable reduction in estimation error and the real-time accuracy of the derived specific-impulse readout.

The remainder of this paper is organized as follows. Section II reviews related work in Kalman-filter sensor fusion and rocket static-fire instrumentation. Section III describes the system architecture. Section IV derives the governing equations of motor performance. Section V presents the sensor-fusion methodology. Section VI describes the simulation setup used for validation. Section VII presents and discusses the results, and Section VIII concludes the paper.

2 RELATED WORK

Kalman-filter sensor fusion is widely used for orientation and navigation estimation from low-cost MEMS sensor suites. Zhang *et al.* proposed a dual-linear Kalman filter that fuses gyroscope, accelerometer, and magnetometer data for real-time orientation determination, reporting a 30.6% reduction in RMS attitude error relative to a conventional single-stage filter [1]. Nemec *et al.* developed an adaptive heterogeneous fusion algorithm for MEMS inertial sensors that converges faster than a fixed-gain extended Kalman filter (EKF), at the cost of a marginally higher steady-state error [2]. These results motivate the trade-off explored in this paper between transient responsiveness and steady-state noise rejection, applied instead to propulsion-performance channels.

In launch-vehicle navigation, Vandersteen *et al.* describe a robust Schmidt–Kalman filter that fuses GNSS and inertial measurements for the Vega launcher, explicitly accounting for parametric sensor uncertainty [3]. Related work in spacecraft attitude and pose estimation applies error-state EKF and invariant-EKF formulations to fuse rate-gyro, accelerometer, and ranging data [4], [6], confirming that Kalman-filter fusion architectures generalize well across aerospace state-estimation problems with heterogeneous sensor suites.

On the instrumentation side, several studies quantify the uncertainty inherent in solid-motor static-fire thrust and pressure measurement. Freeman's thesis on tactical solid-motor test-stand optimization found that load-cell/test-stand structural resonance is the dominant source of thrust-signal distortion, and that a 5,000 lbf thrust measurement could be resolved to within ±0.26% of full scale with proper load-cell stiffness and calibration [9]. Castor *et al.* present a metrological uncertainty analysis of thrust and total-impulse measurement in static rocket-motor firing tests, underscoring that the measurement chain — not just the transducer — governs overall accuracy [10]. These works motivate treating the sensor chain as a whole system to be fused and corrected, rather than trusting any single channel in isolation.

Kalman-filter estimation of an internal thermodynamic state from indirect measurements has precedent outside propulsion: Quartullo *et al.* reconstruct in-cylinder combustion pressure of a diesel engine from rotational-speed measurements alone using an EKF, achieving a fit performance exceeding 90% [8]. Similarly, gas-turbine gas-path health estimation has long used Kalman and hybrid Kalman filters to infer unmeasured internal states from available sensor channels [13], [14]. This paper adapts the same estimation philosophy — inferring a smoothed internal performance state from imperfect, redundant external measurements — to the specific dynamics of a solid rocket motor burn.

The adaptive filtering approach used here builds on the innovation-based adaptive estimation framework introduced by Mehra [12] and applied to INS/GPS integration by Mohamed and Schwarz [11], in which the process-noise covariance is adjusted online based on the whiteness of the innovation sequence rather than fixed a priori. Unlike the sliding-window covariance estimators typically used for continuous adaptation, the present work uses a simpler bounded-hold trigger suited to the discrete, predictable transient structure of a motor burn (ignition and tail-off), which keeps the estimator computationally lightweight enough for embedded real-time implementation.

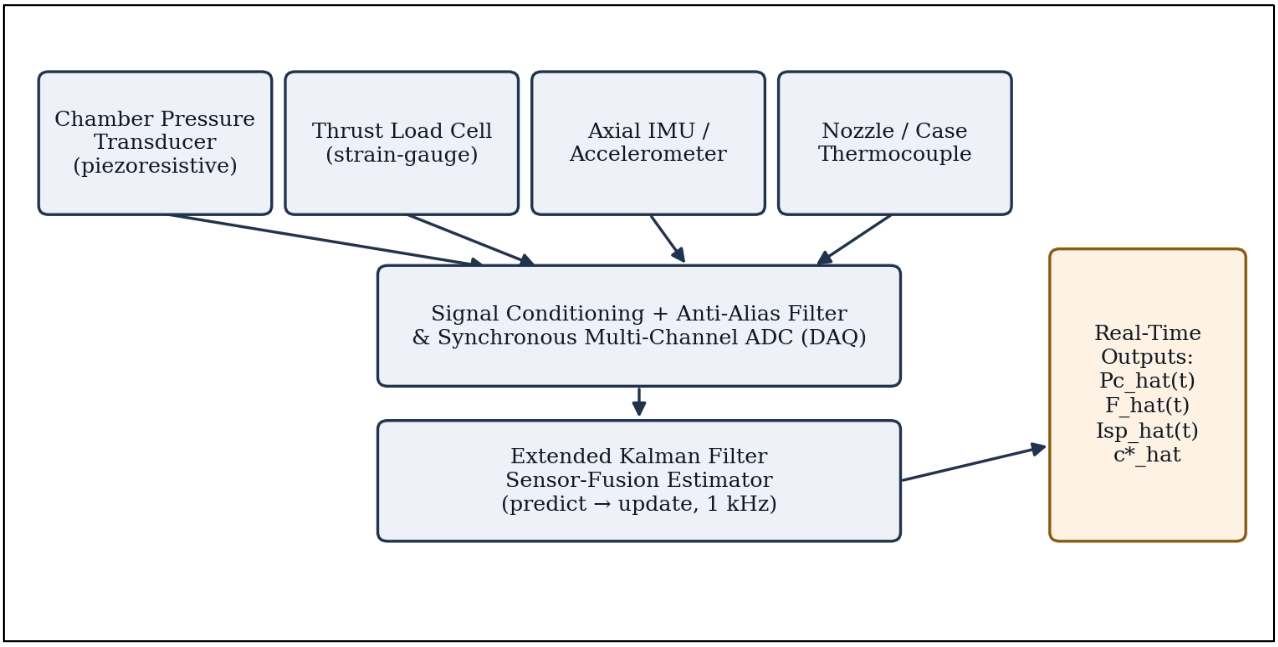

Figure 1: Multi-sensor fusion architecture. Chamber-pressure, load-cell, IMU, and thermocouple channels are conditioned and digitized by a synchronous multi-channel DAQ, then fused by the adaptive Kalman filter to publish real-time chamber pressure, thrust, specific impulse, and characteristic velocity.

3 SYSTEM ARCHITECTURE

Fig. 1 shows the sensor-fusion architecture. Four instrumentation channels are mounted on the static test stand: a piezoresistive chamber-pressure transducer threaded into the forward closure, a strain-gauge thrust load cell in line between the motor mount and the rigid test-stand rail, an axial-axis IMU/accelerometer rigidly bonded to the motor cradle, and a case/nozzle thermocouple for thermal monitoring. All four channels are conditioned (amplification, anti-alias filtering) and digitized by a synchronous multi-channel data-acquisition (DAQ) unit sampling at 1 kHz, which is fast enough to resolve the millisecond-scale ignition transient while remaining within the bandwidth of low-cost 24-bit sigma-delta ADCs.

Table 1: Sensor Suite Specification

Channel	Range	1σ Noise	Rate
Pressure transducer	0–20 MPa	45 kPa	1 kHz
Thrust load cell	0–5 kN	12 N	1 kHz
Axial accelerometer	0–100 g	4.5 m/s^2	1 kHz
Case thermocouple	0–1200 °C	—	100 Hz

The digitized samples are passed to the fusion estimator described in Section V, which runs the predict–update Kalman recursion once per sample and publishes four real-time outputs: fused chamber pressure P_c, fused thrust F, instantaneous specific impulse $I_{sp}(t)$, and characteristic velocity c^*. Table I summarizes the assumed specification of each sensor channel used for the simulation study in Section VI.

4 GOVERNING EQUATIONS OF MOTOR PERFORMANCE

The truth model against which the fusion estimator is validated follows standard solid-motor internal-ballistics relations [16]. The propellant regression rate follows Saint-Robert's burn law,

$r = aP_c^n$, (1)

where a and n are empirically fitted burn-rate coefficients. The rate of gas generation from the burning surface area A_b is

$\dot{m}_{gen} = \rho_p A_b r$, (2)

with propellant density ρ_p. Chamber pressure evolves according to the lumped-parameter chamber-filling equation

$dP_c/dt = (RT_c/V_c)(\dot{m}_{gen} - \dot{m}_{noz}) - P_c/V_c \cdot dV_c/dt$, (3)

where R is the specific gas constant, T_c the adiabatic flame temperature, and V_c the instantaneous free chamber volume. The choked nozzle mass flow is

$\dot{m}_{noz} = P_c A_t \sqrt{[(\gamma/RT_c)\cdot(2/(\gamma+1))^{(\gamma+1)/(\gamma-1)}]}$, (4)

with throat area A_t and specific-heat ratio γ. Thrust is

$F = C_f P_c A_t$, (5)

where the thrust coefficient C_f includes the momentum and pressure-mismatch terms

$C_f = \sqrt{[Y]} + (P_e - P_a)A_e/(P_c A_t)$, (6)

with $Y = [2\gamma^2/(\gamma-1)]\cdot[2/(\gamma+1)]^{(\gamma+1)/(\gamma-1)}\cdot[1-(P_e/P_c)^{(\gamma-1)/\gamma}]$, exit pressure P_e obtained from the isentropic area–Mach relation for the fixed expansion ratio $\varepsilon = A_e/A_t$, and ambient pressure P_a. Characteristic velocity and specific impulse follow as

$c^* = P_c A_t/\dot{m}_{noz}$, $I_{sp} = F/(\dot{m}_{noz} g_0) = C_f c^*/g_0$. (7)

These relations couple P_c and F tightly enough that fusing their independent noisy measurements is physically well motivated: a transient in one channel that is inconsistent with the nozzle relation is, with high probability, sensor noise rather than a true performance change.

5 SENSOR FUSION METHODOLOGY

5.1 State and Measurement Model

A reduced-order state vector $x = [P_c, F]^T$ is used rather than a full internal-ballistics state, since the burn-rate and grain-geometry parameters that drive P_c and F are not independently observable from the available sensor suite in real time. Each state is propagated as a locally constant (random-walk) process between updates,

$\hat{x}_{k|k-1} = \hat{x}_{k-1}$, $P_{k|k-1} = P_{k-1} + Q$, (8)

which is appropriate because the true chamber-pressure and thrust trajectories evolve smoothly on the 10–100 ms combustion time scale, far slower than the 1 kHz sample interval. Three measurements are available per cycle:

$z = [P_{c,meas}, F_{LC}, F_{acc}]^T$, (9)

where F_{LC} is the load-cell reading and $F_{acc} = \hat{a}m(t)$ is thrust inferred from the axial accelerometer and the (known, time-varying) instantaneous motor mass $m(t)$. Because P_c and F are each observed directly, the measurement model is linear, $z = Hx + v$, which keeps the estimator a standard (rather than extended) Kalman filter despite the underlying nonlinear plant.

5.2 Sequential Scalar Update

The three-channel update is implemented as three sequential scalar Kalman updates rather than a single batch vector update. This is algebraically equivalent for uncorrelated measurement noise and avoids ill-conditioned matrix inversion when channel noise variances differ by orders of magnitude (e.g., $\sigma_{Pc} \approx 45$ kPa vs. $\sigma_F \approx 12$ N). For the thrust state, the load-cell update is applied first, followed by the accelerometer-derived update — this second step is the sensor-fusion operation proper, since it combines two physically independent thrust estimates:

$$K_1 = P_F/(P_F+R_{LC}),\ \hat{F} \leftarrow \hat{F}+K_1(F_{LC}-\hat{F}), \qquad (10)$$

$$K_2 = P_F/(P_F+R_{acc}),\ \hat{F} \leftarrow \hat{F}+K_2(F_{acc}-\hat{F}), \qquad (11)$$

with the state covariance P_F reduced by the standard factor $(1-K)$ after each scalar update.

5.3 Innovation-Based Adaptive Process Noise

A fixed process-noise covariance Q forces a compromise between fast transient tracking and steady-state noise rejection. Rather than accept this compromise, the filter monitors the normalized innovation of each channel,

$$\nu_k = z_k - \hat{x}_{k|k-1}, \qquad (12)$$

and compares it against a threshold scaled by the predicted innovation standard deviation. When $|\nu_k|$ exceeds $\eta\sqrt{(P_{k|k-1}+Q+R)}$ for a threshold $\eta = 3$, a transient is declared and Q is inflated by a fixed boost factor for a bounded hold interval (40 ms for the pressure state, 10 ms for the faster-responding thrust state), after which it relaxes back to its tightly tuned steady-burn value. This bounded-hold variant of innovation-based adaptive estimation [11], [12] is deliberately simpler than sliding-window covariance-matching adaptive filters [11]: because a motor burn has only two transients (ignition and tail-off) whose approximate duration is known a priori, a fixed hold interval triggered by innovation is sufficient and keeps the estimator computationally cheap enough for embedded real-time execution. Fig. 2 summarizes the resulting predict–update–adapt cycle.

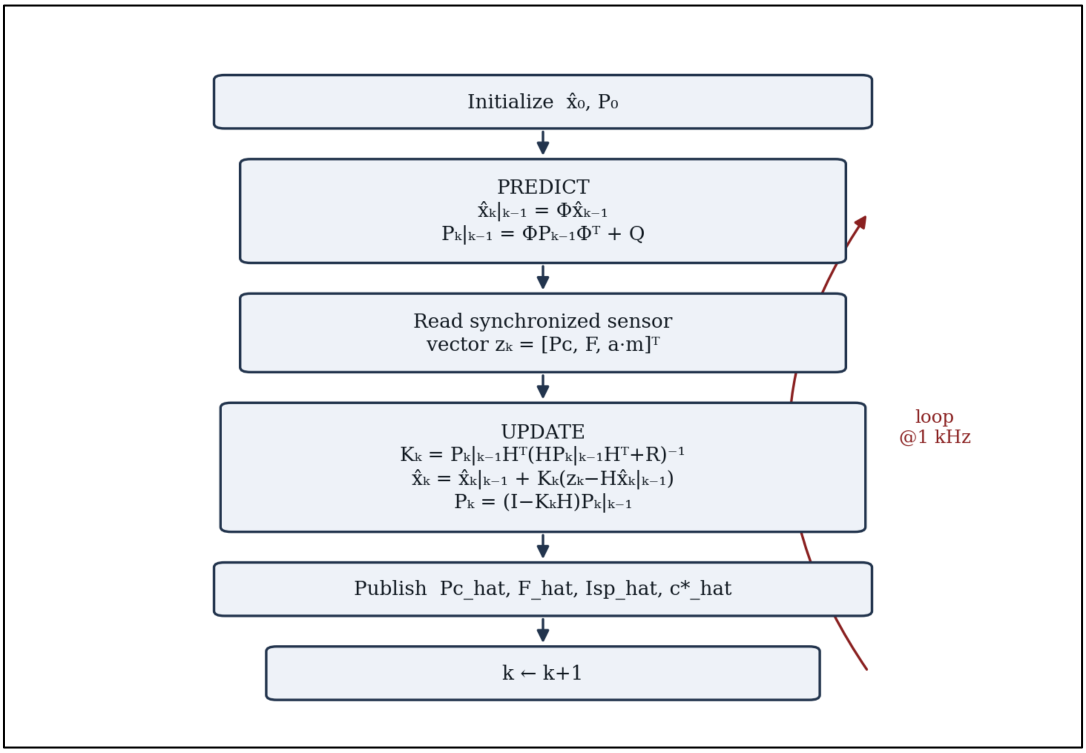

Figure 2: Adaptive Kalman-filter predict–update cycle. The innovation test at each step determines whether the process-noise covariance Q is temporarily inflated to track an ignition or tail-off transient.

6 SIMULATION SETUP

The fusion estimator is validated against a synthetic but physically consistent burn of an AP/HTPB/aluminized composite motor, generated by numerically integrating (2)–(7) at 1 kHz. Table II lists the assumed motor and simulation parameters; Table III lists the sensor-noise parameters used to synthesize each measurement channel from the truth trajectory. The exit Mach number and pressure ratio for the fixed expansion ratio ε = 4.5 are obtained by Newton–Raphson solution of the isentropic area–Mach relation.

Table 2: Motor And Simulation Parameters

Parameter	**Symbol**	**Value**
Propellant density	ρp	1770 kg/m^3
Flame temperature	Tc	3350 K
Specific-heat ratio	γ	1.18
Throat diameter	—	15.3 mm
Expansion ratio	ε	4.5
Burn-rate exponent	n	0.32
Sample rate	—	1 kHz

Table 3: Synthesized Sensor Noise

Channel	**Bias**	**1σ Noise**
Pressure transducer	40 kPa	45 kPa
Thrust load cell	—	12 N
Accelerometer	—	4.5 m/s^2

The load-cell channel additionally includes a decaying 180 Hz structural-ringing artifact at ignition, consistent with the resonance behavior reported for test-stand/load-cell assemblies in static-fire uncertainty studies [9]. The resulting truth burn reaches a peak chamber pressure of 11.8 MPa and peak thrust of 3480 N over a 2.44 s burn, with a burn-averaged specific impulse of 270 s and total impulse of 6833 N·s, all consistent with a small AP/HTPB/Al composite motor of this scale.

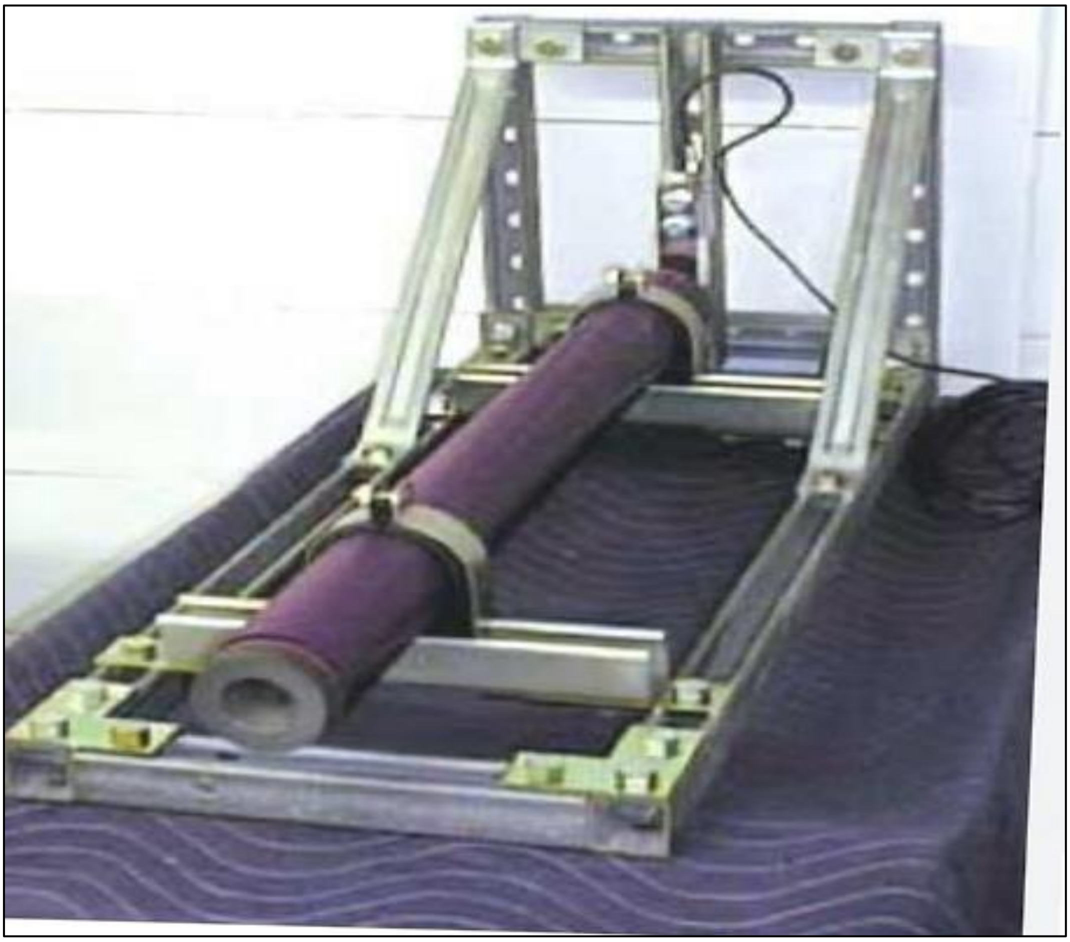

Figure 3: Static test-stand instrumentation layout. The motor is rigidly mounted on the thrust rail with an in-line load cell, forward-closure pressure transducer, axial IMU, and case thermocouple, all routed to the multi-channel DAQ and real-time fusion PC.

7 RESULTS

7.1 Chamber Pressure and Thrust Reconstruction

Fig. 3 compares the raw pressure-transducer reading, the true chamber-pressure trajectory, and the fused estimate. The adaptive filter tracks the ignition rise and tail-off fall within a few samples while visibly suppressing the sensor noise during the quasi-steady burn. Across the metric window (thrust above 5% of peak), the fused estimate reduces pressure RMS error from 59.1 kPa (raw) to 45.9 kPa — a 22.2% reduction. Fig. 4 shows the corresponding thrust reconstruction, fusing the raw load-cell signal with the independent accelerometer-derived channel; thrust RMS error falls from 12.4 N (raw load cell) to 7.5 N, a 39.0% reduction, with the larger gain reflecting the added information from the second, independent thrust-observing channel that has no analogue on the pressure side.

7.2 Real-Time Specific Impulse

Fig. 5 shows the real-time $I_{sp}(t)$ computed from the fused P_c and F estimates against the instantaneous true value. During the quasi-steady burn (0.3–2.0 s) the real-time estimate has a mean of 270.15 s against a true burn-averaged I_{sp} of 270.21 s — a difference of 0.02% — demonstrating that the fused channels are consistent enough to support real-time performance-margin decisions without waiting for post-fire data reduction.

7.3 Adaptive Covariance Behavior

Fig. 6 plots the 1σ uncertainty of each state over the burn. The characteristic spikes correspond to innovation-triggered Q inflation: the pressure-state uncertainty spikes to ≈38 kPa whenever the filter detects a transient, then relaxes to ≈21 kPa during quasi-steady tracking; the thrust-state uncertainty follows the same pattern between ≈6.7 N and ≈10.7 N. The largest and most closely spaced spikes occur during tail-off (2.2–2.5 s), reflecting the rapidly changing burning-surface area as the grain sliver is consumed.

7.4 Performance Summary

Table 4: Summary Of Estimation Performance

Metric	Raw	Fused
Pc RMSE	59.1 kPa	45.9 kPa
F RMSE	12.4 N	7.5 N
Isp error (quasi-steady)	—	0.02%
Peak Pc	11.8 MPa	—
Peak F / Total impulse	3480 N / 6833 N·s	—

8 DISCUSSION AND LIMITATIONS

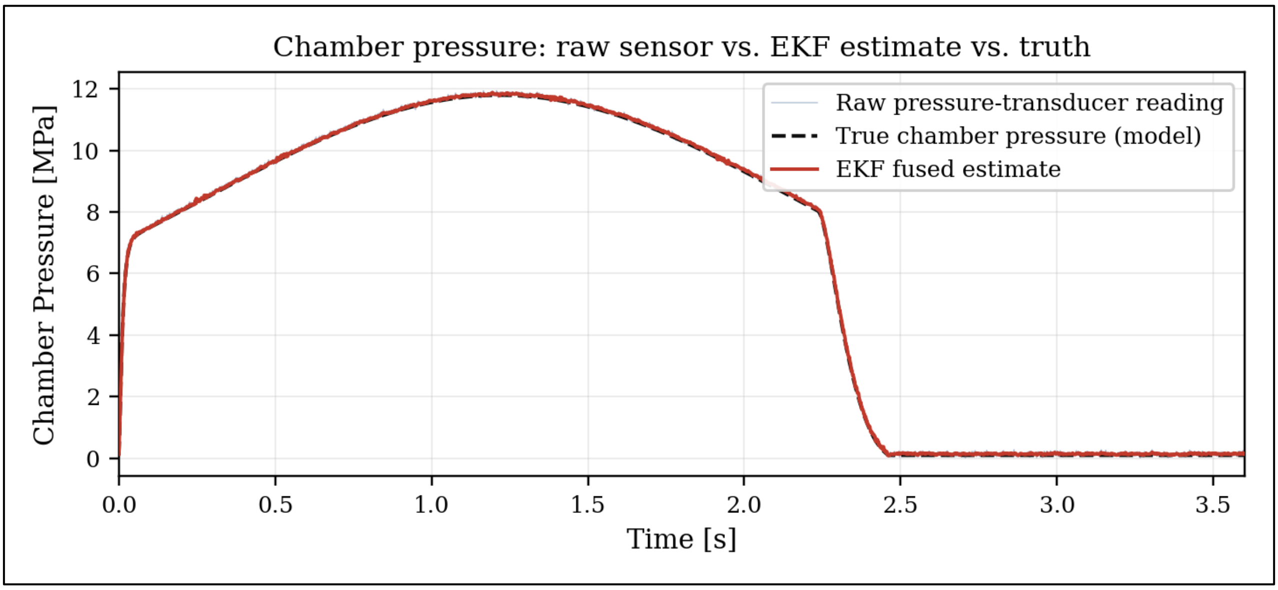

Figure 4: Chamber pressure: raw transducer reading, true simulated trajectory, and adaptive-KF fused estimate.

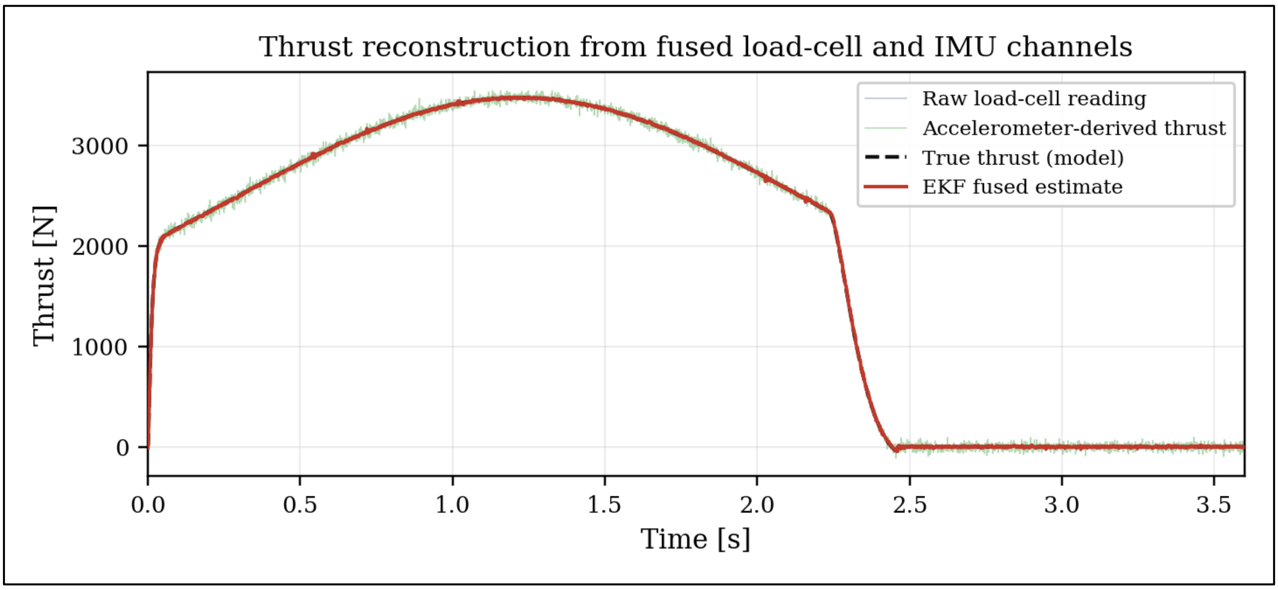

Figure 5: Thrust: raw load-cell reading, accelerometer-derived channel, true trajectory, and fused estimate.

The reduced-order [P_c, F] state was chosen because burn-rate and grain-geometry parameters are not independently observable from the assumed sensor suite; a richer state including mass flow or burning-surface area would require either an additional observable (e.g., optical grain-regression tracking) or a physics-embedded process model, at the cost of the linear-Gaussian simplicity exploited here. The synthetic sensor noise, while parameterized from published static-fire uncertainty studies [9], [10], does not capture every real-world error source — electromagnetic interference from igniter circuits, thermal drift of the pressure transducer over the burn duration, and cross-axis vibration coupling into the accelerometer channel are all first-order effects in a physical test stand that a hardware implementation would need to characterize and, where necessary, fold into the measurement-noise covariance R. The bounded-hold adaptive scheme is also tuned to the two-transient structure of a single burn; a motor with pressure oscillations (combustion instability) would require either a shorter hold interval or a continuously adaptive covariance-matching scheme such as [11].

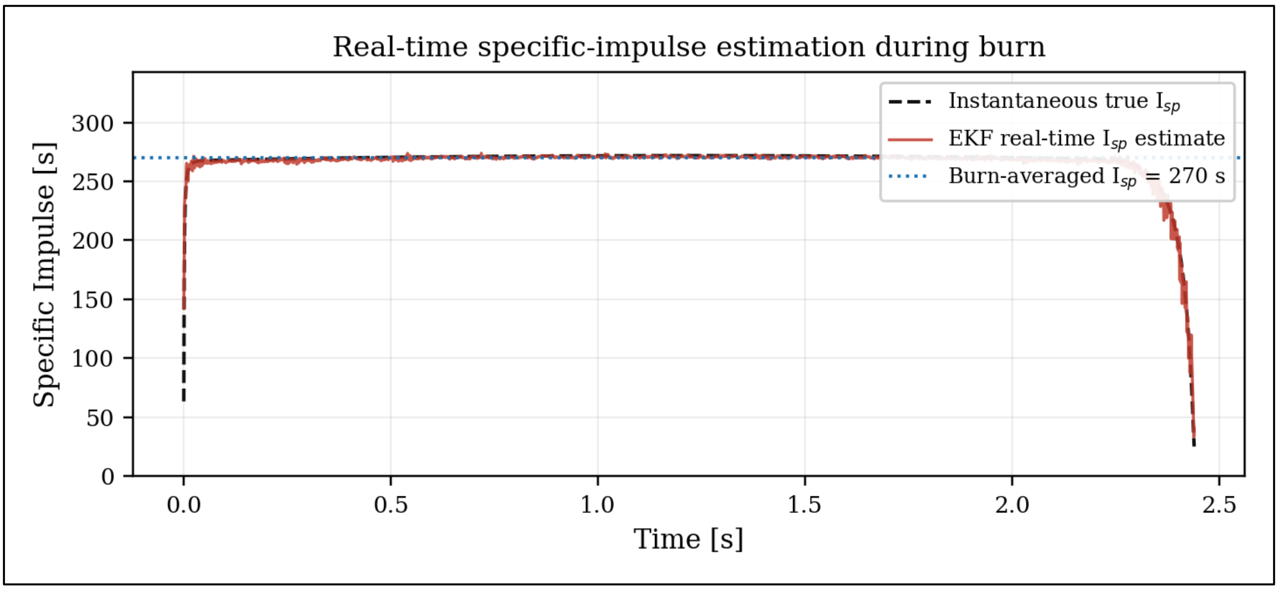

Figure 6: Real-time specific-impulse estimate vs. instantaneous true value and the burn-averaged reference.

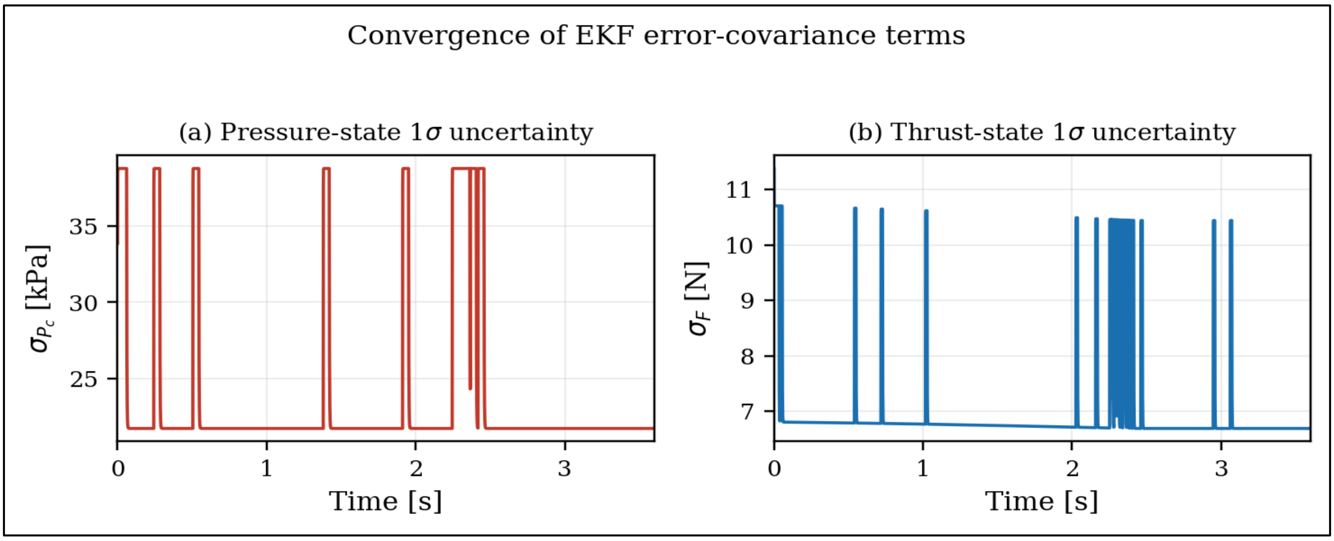

Figure 7: Convergence and transient re-inflation of the adaptive filter's 1σ error-covariance terms for the pressure and thrust states.

9 CONCLUSION

This paper presented a real-time multi-sensor fusion architecture for solid rocket motor performance estimation, combining chamber-pressure, load-cell, and accelerometer-derived thrust channels through an adaptive Kalman filter with innovation-triggered process-noise inflation. Validated against a physically grounded internal-ballistics truth model, the fused estimator reduced chamber-pressure RMS error by 22.2% and thrust RMS error by 39.0% relative to raw sensor channels, and reconstructed real-time specific impulse to within 0.02% of the true burn-averaged value during the quasi-steady burn phase. The bounded-hold adaptive scheme resolved the transient-tracking/noise-rejection trade-off inherent to fixed-gain filtering without increasing state-vector complexity, making it suitable for low-cost, embedded real-time implementation on a static test stand.

FUTURE WORK

Future work includes hardware-in-the-loop validation on a physical static test stand to characterize real sensor error sources (EMI, thermal drift, vibration coupling) not captured by the synthetic noise model; extension of the state vector to include burning-surface area or mass flow using an embedded physics-based process model; application of covariance-matching adaptive estimation for motors exhibiting combustion instability; and extension of the fusion architecture from static ground testing to flight telemetry, incorporating barometric altitude and GNSS-derived acceleration alongside onboard pressure and IMU channels for in-flight motor-performance monitoring.

STATEMENTS ON COMPLIANCE WITH ETHICAL STANDARDS

Acknowledgments

To everyone who contributed to this achievement, I sincerely say thank you. This success is a reflection of collective effort, dedication, and perseverance.

Disclosure of conflict of interest

There is no conflict of interest to be disclosed.

REFERENCES

[1] S. Zhang, S. Yu, C. Liu, X. Yuan, and S. Liu, "A dual-linear Kalman filter for real-time orientation determination system using low-cost MEMS sensors," Sensors, vol. 16, no. 2, art. 264, Feb. 2016.

[2] D. Nemec, A. Janota, M. Hruboš, and V. Šimák, "Intelligent real-time MEMS sensor fusion and calibration," arXiv:1701.07594, Jan. 2017.

[3] J. Vandersteen, S. Bennani, and C. Roux, "Robust rocket navigation with sensor uncertainties: Vega launcher application," J. Spacecraft and Rockets, vol. 55, no. 1, pp. 153–166, 2018.

[4] X. Ye, F. Song, Z. Zhang, R. Zhang, and Q. Zeng, "Semi-aerodynamic model aided invariant Kalman filtering for UAV full-state estimation," arXiv:2310.01844, Oct. 2023.

[5] C. Lee, "Observability decomposition-based decentralized Kalman filter and its application to resilient state estimation under sensor attacks," Sensors, vol. 22, no. 18, art. 6909, Sep. 2022.

[6] D. Parikh and M. Majji, "Pose estimation of CubeSats via sensor fusion and error-state extended Kalman filter," arXiv:2409.10815, Sep. 2024.

[7] I. Miloud, S. Cauet, E. Etien, J. P. Salameh, and A. Ungerer, "Real-time speed estimation for an induction motor: An automated tuning of an extended Kalman filter using voltage–current sensors," Sensors, vol. 24, no. 6, art. 1744, Mar. 2024.

[8] R. Quartullo, A. Garulli, A. Giannitrapani, R. Minamino, and G. Vichi, "In-cylinder pressure estimation from rotational speed measurements via extended Kalman filter," Sensors, vol. 23, no. 9, art. 4326, Apr. 2023.

[9] C. W. Freeman II, "Solid rocket motor static fire test stand optimization: Load cell effects and other uncertainties," M.S. thesis, Dept. Mech. Aerosp. Eng., Univ. of Alabama in Huntsville, Huntsville, AL, USA, 2018.

[10] F. de P. L. Castor, C. R. Hall Barbosa, and E. C. de Oliveira, "Assessing the metrological reliability of static firing tests of rocket motors through the evaluation of thrust and total impulse measurement uncertainty," Appl. Sci., vol. 15, no. 8, art. 4280, Apr. 2025.

[11] A. H. Mohamed and K. P. Schwarz, "Adaptive Kalman filtering for INS/GPS," J. Geodesy, vol. 73, no. 4, pp. 193–203, May 1999.

[12] R. K. Mehra, "Approaches to adaptive filtering," IEEE Trans. Autom. Control, vol. 17, no. 5, pp. 693–698, Oct. 1972.

[13] B. Pourbabaee, N. Meskin, and K. Khorasani, "Sensor fault detection, isolation, and identification using multiple-model-based hybrid Kalman filter for gas turbine engines," IEEE Trans. Control Syst. Technol., vol. 24, no. 4, pp. 1184–1200, Jul. 2016.

[14] F. Lu, Y. Wang, J. Huang, Y. Huang, and X. Qiu, “Fusing unscented Kalman filter for performance monitoring and fault accommodation in gas turbine,” Proc. Inst. Mech. Eng., Part G: J. Aerosp. Eng., vol. 232, no. 3, pp. 556–570, 2018.

[15] R. E. Kalman, “A new approach to linear filtering and prediction problems,” Trans. ASME J. Basic Eng., vol. 82, no. 1, pp. 35–45, 1960.

[16] G. P. Sutton and O. Biblarz, Rocket Propulsion Elements, 9th ed. Hoboken, NJ, USA: Wiley, 2017.